Tropical modulation of East Asia air pollution

Myung-Il Jung
Seoul National University
Seok-Woo Son (seokwooson@snu.ac.kr)
Seoul National University
Hyemi Kim
Stony Brook University https://orcid.org/0000-0003-4713-4658
Deliang Chen
University of Gothenburg https://orcid.org/0000-0003-0288-5618

Article

Keywords: PM10, East Asia, Madden-Julian oscillation, tropical-extratropical teleconnection

Posted Date: December 22nd, 2020

DOI: https://doi.org/10.21203/rs.3.rs-117130/v1

Version of Record: A version of this preprint was published at Nature Communications on September 23rd, 2022. See the published version at https://doi.org/10.1038/s41467-022-33281-1.

Tropical modulation of East Asia air pollution

Myung-Il Jung[a], Seok-Woo Son[a,*], Hyemi Kim[b], and Deliang Chen[c]

[a]School of Earth and Environmental Sciences, Seoul National University, Seoul, South Korea

[b]School of Marine and Atmospheric Sciences, Stony Brook University, State University of New York, Stony Brook, New York, USA

[c]Department of Earth Sciences, University of Gothenburg, Gothenburg, Sweden

November 2020

Submitted to *Nature Geoscience*

*Corresponding author: Seok-Woo Son, School of Earth and Environmental Sciences, Seoul National University, 1 Gwanak-ro, Gwanak-gu, Seoul, 08826, South Korea

E-mail: seokwooson@snu.ac.kr

Abstract

Given the high population density and serious air pollution problems, understanding and predicting air pollution in East Asia are of great importance. Here, we show that the day-to-day variability of East Asia air pollution in winter is remotely controlled by the convection over the tropical Indian Ocean and western Pacific, the so-called Madden–Julian oscillation (MJO), through its extratropical teleconnections. In particular, the concentration of particulate matter with aerodynamic diameter less than 10 micron (PM_{10}) becomes significantly high when the tropical convection is suppressed over the Indian Ocean (MJO phases 5–6). In contrast, PM_{10} concentration becomes significantly low when the convection is enhanced there (MJO phase 1–2). The station-averaged PM_{10} difference between the two MJO phases reaches up to 47% of the daily PM_{10} variability, indicating that the MJO is a primary source of wintertime subseasonal variability of East Asia PM_{10} concentration. We also show that PM_{10} anomaly typically lags the tropical convection by one to two weeks. This opens a new window of opportunity for subseasonal PM_{10} prediction in East Asia.

Keywords: PM_{10}, East Asia, Madden-Julian oscillation, tropical-extratropical teleconnection

Main

Severe air pollution events, with high PM_{10} concentration, have frequently occurred in East Asia over past decades, despite the government's air quality regulation[1–3]. Such events, which are most frequent in cold season[4], have often been explained by local emissions and meteorological conditions that control aerosol deposition, accumulation, and transport[5,6]. Although minor, they are also influenced by climate variability on a wide range of time scales. On the interannual time scale, for instance, wintertime PM_{10} level in East Asia is weakly sensitive to the El Nino–Southern Oscillations (ENSO)[7] and the Arctic sea ice variability[8,9]. The relationship between haze days and Pacific Decadal Oscillation (PDO)[10,11] also implies that PM_{10} may be affected by climate oscillation on the decadal time scale.

On the daily time scale, East Asia PM_{10} substantially varies. In this study, we show that its daily variability is not random but significantly influenced by subseasonal climate variability in the tropics. Specifically, we show that the wintertime PM_{10} variability is to a large extent determined by the tropical climate variability, referred to as the Madden-Julian oscillation (MJO)[12,13]. The MJO is a planetary-scale convection–circulation coupled system in the tropics that typically moves eastward from the tropical Indian Ocean to the western Pacific with a period of 30 to 60 days. Although organized in the tropics, its impacts are not limited to the tropics. As the MJO propagates, it influences the midlatitude circulation by exciting the Rossby wave train[14,15]. Over East Asia, which is on the main pathway of the Rossby wave train, precipitation, temperature, and atmospheric circulations are significantly modulated by the MJO[16–18], affecting local air pollution.

MJO-related East Asia PM_{10} change

Figure 1a presents PM_{10} climatology in China and Korea during the boreal winter (December-February). The overall PM_{10} level, ranging from 30 $\mu g\ m^{-3}$ to 200 $\mu g\ m^{-3}$, is relatively high compared to that in Europe and North America[19]. Urban areas in northern China, including Beijing, whose PM_{10} level is determined by industrial emissions, residential heating, and transportation, show particularly higher values

than rural areas in southern China. Most monitoring stations in Korea exhibit relatively low PM_{10} concentration than those in China, but megacities such as Seoul still show a high PM_{10} concentration.

The daily PM_{10} variability is quantified in Fig. 1b by computing daily one standard deviation. The overall variability, averaged over the analysis domain, is 28 μg m^{-3}. This value accounts for 29% of the daily climatology, indicating a significant day-to-day variability of East Asia PM_{10}, especially at the stations with a high PM_{10} climatology in northern China. Approximately 30% to 60% of the daily variability is due to subseasonal variability, derived from a 20–96 day band-pass-filtered PM_{10} anomaly (Fig. 1c). Such a large contribution of the subseasonal PM_{10} variation, particularly in southeastern China and Korea, cannot be explained by local emissions alone. It can be also associated with meteorological conditions.

On the subseasonal timescale, midlatitude atmospheric circulation is influenced not only by local processes but also by remote processes. One of the most important remote processes that determine the atmospheric circulation in East Asia is the tropical–extratropical teleconnections driven by the MJO[14]. By exciting the Rossby gyres in the subtropics and the Rossby waves that propagate into the midlatitude[14,15], the MJO effectively modulates the precipitation and atmospheric circulation in the midlatitude. It is well documented that winter precipitation in East Asia, especially in southern China, Korea, and western Japan, increases when the MJO convection is enhanced over the tropical Indian Ocean but suppressed over the western Pacific (MJO phase 1–2; Fig. 2c). The opposite is true when the MJO convection is suppressed over the tropical Indian Ocean but enhanced over the western Pacific (MJO phase 5–6; Fig. 2d).

The MJO-related precipitation and atmospheric circulation anomalies significantly modulate the wintertime PM_{10} concentration in East Asia. Figures 2a and b show subseasonal PM_{10} anomalies during MJO phases 1–2 and 5–6 at lag 6 to 10 days (i.e., 6–10 days after the selected MJO phase). During MJO phase 1–2, PM_{10} concentration becomes anomalously low almost everywhere except in northeastern China (Fig. 2a). The station-averaged PM_{10} anomaly is approximately -5 μg m^{-3}, being statistically significant at the 95% confidence level. In contrast, PM_{10} concentration is anomalously high during MJO phase 5–6 (Fig. 2b). Their spatial distribution is almost identical to that during MJO phase 1–2, but with an opposite sign

98 (see Extended Data Fig. 1 for the other MJO phases). The station-averaged PM_{10} anomaly of approximately
99 6 μg m^{-3} is also comparable to that in MJO phase 1–2.

100 This mirroring result indicates that the MJO systematically modulates PM_{10} concentration in East Asia.
101 When considering the unfiltered PM_{10} anomaly (Extended Data Fig. 2), the station-averaged PM_{10}
102 difference between MJO phases 1–2 and 5–6, which is greater than 10 μg m^{-3}, is up to 47% of daily PM_{10}
103 variability (~28 μg m^{-3}).

104 The temporal evolution of the station-averaged PM_{10} anomaly is further examined by considering eight
105 MJO phases (Extended Data Fig. 3a). Not surprisingly, it follows well the evolution of the MJO convection
106 with a maximum value at lag 6 to 10 days (Extended Data Fig. 3b). This time lag matches with the time
107 scale by which the MJO-induced Rossby waves take to affect in the midlatitude[20,21]. This accentuates the
108 importance of the MJO in subseasonal PM_{10} variability in East Asia.

109 The MJO also modulates high PM_{10} days. Figure 3 shows the frequency distribution of the station-
110 averaged PM_{10} concentration. No time filtering is applied here. The frequency distribution exhibits a long
111 tail with increasing PM_{10} concentration (Fig. 3a), indicating that high pollution days occur more frequently
112 than clean air days. A similar frequency distribution, with different mean and extremes, is also found when
113 MJO phases 1–2 and 5–6 are separately considered (Fig. 3b). The PM_{10} concentration during MJO phase
114 1–2 is on average around 88 μg m^{-3}, which is 10% smaller than the winter average of about 98 μg m^{-3}.
115 However, the PM_{10} concentration during MJO phase 5–6 is biased toward the higher values, with its mean
116 value of about 103 μg m^{-3}. This is approximately 1.2 times higher than that during MJO phase 1–2. This
117 result is consistent with Fig. 2 which is based on subseasonally-filtered PM_{10} anomalies. It is evident from
118 Fig. 3b that the PM_{10} distribution is skewed toward high pollution days during MJO phase 5–6. High PM_{10}
119 days, defined as days with PM_{10} concentration greater than 140 μg m^{-3} corresponding to the top 10 percentile,
120 are more frequently observed during MJO phase 5–6. This result indicates that the MJO teleconnections
121 modulate not only the mean PM_{10} concentration but also the frequency of high PM_{10} days in East Asia.
122

How does the MJO modulate East Asia PM_{10}?

The MJO-related PM_{10} anomalies likely result from the changes in regional precipitation and atmospheric ventilations. The enhanced convection over the tropical Indian Ocean during MJO phase 1–2 yields the subtropical Rossby gyre and excites the Rossby wave train toward midlatitudes[22,23]. They strengthen moisture transport and vertical motion in East Asia, leading to more frequent precipitation events (Fig. 2c). Since precipitation can remove PM_{10} via wet scavenging processes[24], it is natural to anticipate reduced PM_{10} during MJO phase 1–2. The positive precipitation frequency anomalies (Fig. 2c) indeed match well with PM_{10} anomalies, especially in southeastern China (Fig. 2a).

During MJO phase 5–6, precipitation events become less frequent in East Asia (Fig. 2d). The opposite precipitation anomaly, compared to MJO phase 1-2, is explained by systematic atmospheric circulation change via the MJO teleconnections. This contributes to anomalously high PM_{10} concentration (Fig. 2b). However, this may not be a sufficient to produce high PM_{10} days as a relatively dry condition itself does not guarantee more frequent high PM_{10} days. Other factors such as atmospheric ventilation changes may also play a role[8,25].

Consistent with previous studies, anticyclonic anomaly is observed in the mid-troposphere from eastern China to Korea during MJO phase 5–6 (Fig. 4a). This circulation anomaly, which is a part of the Rossby gyre, drives anomalous downward motion that promotes the accumulation of local pollutants[6]. The anticyclonic anomaly can also enhance the atmospheric stratification near the surface. The bulk stability, which is defined by the potential temperature difference between 925 and 1000 hPa, is indeed enhanced, especially in eastern China (Fig. 4b). The stable boundary layer can lead to reduce vertical ventilation, increasing PM_{10} concentration[8,9]. Horizontal ventilation also becomes weak as evidenced by the weak surface wind (Fig. 4c). All of these circulation patterns suggest that relatively high PM_{10} concentration in East Asia during MJO phase 5–6 is likely caused by the combined effects of less frequent precipitation events and reduced atmospheric ventilations. The atmospheric circulation anomalies opposite to these are observed during MJO phase 1–2 (Extended data Fig. 4). This indicates that low PM_{10} anomaly in Fig. 2a is

148 also partly influenced by the enhanced atmospheric ventilations besides reduced precipitation.

149

150 **Implication to PM_{10} prediction**

151 This study reveals that the winter PM_{10} concentration in East Asia is significantly modulated by the
152 MJO. Specifically, MJO phase 1–2 tends to lead to reduced PM_{10} concentration, presumably due to more
153 frequent precipitation event in East Asia. In contrast, during MJO phase 5–6, PM_{10} concentration becomes
154 anomalously high possibly due to less frequent precipitation event and weak atmospheric ventilation. This
155 finding is all based on the time average from lag 6 to 10 days (Figs. 2–4), the former lagging the latter. This
156 time lag suggests that East Asia PM_{10} can be predicted at least one week in advance by considering the state
157 of the MJO. For instance, it is anticipated that when MJO phase 5–6 is detected in the tropics, the PM_{10} in
158 East Asia increases with a high chance of heavy pollution days one to two weeks later. Since numerical
159 models are capable of predicting the MJO for two to three weeks in advance[26,27], the MJO–PM_{10} connection
160 reported in this study can open a new window of opportunity for subseasonal PM_{10} prediction in East Asia.

161 Given the high population density and serious air pollution problems in East Asia, any added
162 competency to PM_{10} prediction is of great significance. Nevertheless, the results presented here need to be
163 interpreted with caution because of a number of limitations. First, PM_{10} data in China are partly derived
164 from the air pollution index[28]. The data conversion may have introduced small but non-negligible biases.
165 Second, PM_{10} data are available only for 18 years from 2001 to 2018. This is a rather short-term record,
166 compared to long-term meteorological observations commonly used in the MJO teleconnection studies. To
167 better quantify the MJO–PM_{10} relationship, longer data records are required. Third, the effects of local
168 emissions and regional transports are indirectly removed by filtering PM_{10} data with a 20–96 day band-
169 pass-filter. Although this filtering is commonly used in MJO studies, it does not fully eliminate local and
170 regional effects. To isolate the MJO–teleconnection impacts, it may be useful to employ numerical
171 modeling in which the local processes can be controlled.

172

Methods

Observation and Reanalysis Data

Daily PM_{10} concentrations are obtained from air quality monitoring stations in Korea and China for 18 years (2001-2018). The Korean data are directly obtained from the Ministry of Environment, Republic of Korea (https://www.airkorea.or.kr), while the Chinese data are collected from two different sources. Until December 2012, PM_{10} in China is estimated by converting the air pollution index[28,29]. The derived PM_{10} concentrations are quantitatively similar to in-situ measurements[30] and have been widely used in literature as an observations[31]. After December 2013, PM_{10} data are collected from the Air Quality Inspection Platform of China (http://www.aqistudy.cn/historydata/). It may be noted that no data are available in China for 11 months from January to November 2013.

For both the Korean and Chinese stations, only those that exceed 75% of the temporal coverage are considered. This allows inclusion of a total of 100 stations, with 58 in Korea and 42 in China. Because Korean stations are densely distributed, only six stations (i.e., Busan, Daejeon, Gangneung, Gwangju, Jeju, and Seoul) are subsampled when computing the station-averaged PM_{10} concentration.

The daily meteorological variables, including geopotential height, wind, and temperature, are obtained from European Centre for Medium Range Weather Forecasts Reanalysis 5 (ERA5)[32]. The gauge-based precipitation data from the Climate Prediction Center (CPC) (https://ftp.cpc.ncep.noaa.gov/precip/CPC_UNI_PRCP/) and the outgoing longwave radiation (OLR) data from the National Oceanic and Atmospheric Administration (NOAA) (https://psl.noaa.gov/data/gridded/data.interp_OLR.html) are also used. All variables are linearly interpolated into a horizontal resolution of 0.5° longitude x 0.5° latitude.

The daily climatology of each variable is derived from a 31-day moving average of the calendar day mean over 18 years. The anomaly is then calculated by subtracting the daily climatology from the raw data. To focus on the subseasonal variability, the low-frequency anomaly is further isolated by applying a 20–96 day Lanczos band-pass-filter to the daily anomaly. This anomaly, which is referred to as the subseasonal

anomaly, is used in the composite analysis. The statistical significance of the composite value is tested using Student's t-test with the degree of freedom often used in the MJO analysis[33]. The null hypothesis is that the population mean is zero.

Only the boreal winter (December to February) is considered in this study. When considering the extended winter, the overall results do not change much although some results become slightly weak. There is also no noticeable difference when detrended data are used.

MJO index and precipitation frequency index

The OLR-based MJO index (OMI)[34] is utilized in this study. This index is directly obtained from NOAA website (https://www.psl.noaa.gov/mjo/mjoindex/). The MJO phase is defined with the two leading principal components (PC) timeseries, which are calculated by projecting 20–96 day filtered OLR anomalies over 20° S–20° N onto the two leading empirical orthogonal functions. Following previous studies, the MJO phase is divided into eight phases, depending on the location of OLR anomalies. The MJO amplitude is defined as $\sqrt{\mathrm{PC1}^2 + \mathrm{PC2}^2}$. Only well-organized MJO days, with the MJO amplitude greater than one, are considered in the composite analysis. Approximately 63% of days in the analysis period are classified as MJO days.

To relate PM_{10} concentration to precipitation event, the precipitation frequency index is defined. It is counted as one if the daily precipitation exceeds 0.1 mm day^{-1}, otherwise, it is set to zero. Although not shown, the key results are not sensitive to the choice of precipitation threshold varying from 0.1 to 5 mm day^{-1}. It is considered that more frequent precipitation (or a higher precipitation index) is associated with a lower PM_{10} concentration.

Data availability

Daily PM_{10} data of Korea are obtained from the Ministry of Environment, Republic of Korea (https://www.airkorea.or.kr). Chinese PM_{10} data are collected from the air quality index website

(https://aqicn.org/city/) and the Air Quality Inspection Platform of China (https://www.aqistudy.historydata/). The meteorological variables are downloaded from the ERA5 website (https://cds.climate.copernicus.eu/#!/search?text=ERA5&type=dataset). Gauge-based precipitation data from CPC (https://ftp.cpc.ncep.noaa.gov/precip/CPC_UNI_PRCP/) and OLR data from NOAA (https://psl.noaa.gov/data/gridded/data.interp_OLR.html) are available online. The OMI index is also available online (https://www.psl.noaa.gov/mjo/mjoindex/).

Acknowledgments

We thank H. Liao and R. Park for their helpful inputs through discussions. This study was funded by the Korea Meteorological Administration Research and Development Program under Grant KMI2018–01112 and KMI2018–01011. H. Kim was supported by the Brain Pool program funded by the Ministry of Science and ICT through the National Research Foundation of Korea 2019H1D3A2A01102234 and by NSF grant AGS–1652289.

Author contributions

M.-I. J. prepared all the figures, initial draft, and wrote the main manuscript. S.-W. S. initiated the main idea, supervised the work and developed the manuscript. H. K. contributed to the manuscript preparation and provided critical insights on the analysis. D. C. contributed to the interpretation of the result.

Competing interests

The authors declare no competing interests.

References

1. Cai, W., Li, K., Liao, H., Wang, H. & Wu, L. Weather conditions conducive to Beijing severe haze more frequent under climate change. *Nat. Clim. Change* **7,** 257–262 (2017).
2. Kim, H. *et al.* Recent increase of surface particulate matter concentrations in the Seoul Metropolitan Area, Korea. *Sci. Rep.* **7,** 4710 (2017).
3. Shao, P. *et al.* Characterizing remarkable changes of severe haze events and chemical compositions in multi-size airborne particles (PM_1, $PM_{2.5}$ and PM_{10}) from January 2013 to 2016–2017 winter in Beijing, China. *Atmos. Environ.* **189,** 133–144 (2018).
4. Zhang, Y.-L. & Cao, F. Fine particulate matter ($PM_{2.5}$) in China at a city level. *Sci. Rep.* **5,** 14884 (2015).
5. Jeong, J. I. & Park, R. J. Winter monsoon variability and its impact on aerosol concentrations in East Asia. *Environ. Pollut.* **221,** 285–292 (2017).
6. Jung, M.-I. *et al.* Contrasting synoptic weather patterns between non-dust high particulate matter events and Asian dust events in Seoul, South Korea. *Atmos. Environ.* **214,** 116864 (2019).
7. Wie, J. & Moon, B.-K. ENSO-related PM_{10} variability on the Korean Peninsula. *Atmos. Environ.* **167,** 426–433 (2017).
8. Zou, Y., Wang, Y., Zhang, Y. & Koo, J.-H. Arctic sea ice, Eurasia snow, and extreme winter haze in China. *Sci. Adv.* **3,** e1602751 (2017).
9. Kim, J.-H. *et al.* Possible link between Arctic sea ice and January PM_{10} concentrations in South Korea. *Atmosphere* **10,** 619 (2019).
10. Mao, L. *et al.* An observation-based perspective of winter haze days in four major polluted regions of China. *Nati. Sci. Rev.* **6,** 515–523 (2018).
11. Zhao, S., Li, J. & Sun, C. Decadal variability in the occurrence of wintertime haze in central eastern China tied to the Pacific Decadal Oscillation. *Sci. Rep.* **6,** 27424 (2016).

12. Madden, R. A. & Julian, P. R. Detection of a 40–50 day oscillation in the zonal wind in the tropical Pacific. *J. Atmos. Sci.* **28,** 702–708 (1971).

13. Madden, R. A. & Julian, P. R. Description of global-scale circulation cells in the tropics with a 40–50 day period. *J. Atmos. Sci.* **29,** 1109–1123 (1972).

14. Zhang, C. Madden–Julian Oscillation: Bridging weather and climate. *Bull. Amer. Meteor. Soc.* **94,** 1849–1870 (2013).

15. Stan, C. *et al.* Review of tropical–extratropical teleconnections on intraseasonal time scales. *Rev.Geophys.* **55,** 902–937 (2017).

16. Jeong, J.-H., Ho, C.-H., Kim, B.-M. & Kwon, W.-T. Influence of the Madden-Julian Oscillation on wintertime surface air temperature and cold surges in East Asia. *J. Geophys. Res. Atmos.* **110,** D11104 (2005).

17. Seo, K.-H., Lee, H.-J. & Frierson, D. M. W. Unraveling the teleconnection mechanisms that induce wintertime temperature anomalies over the Northern Hemisphere continents in response to the MJO. *J. Atmos. Sci.* **73,** 3557–3571 (2016).

18. Kim, H., Son, S.-W. & Yoo. C. QBO modulation of the MJO-related precipitation in East Asia. *J. Geophys. Res. Atmos.* **125,** e2019JD031929 (2020).

19. Mukherjee, A. & Agrawal, M. World air particulate matter: sources, distribution and health effects. *Environ. Chem. Lett.* **15,** 283–309 (2017).

20. Hoskins, B. J. & Karoly, D. J. The steady linear response of a spherical atmosphere to thermal and orographic forcing. *J. Atmos. Sci.* **38,** 1179–1196 (1981).

21. Jin, F. & Hoskins, B. J. The direct response to tropical heating in a baroclinic atmosphere. *J. Atmos. Sci.* **52,** 307–319 (1995).

22. Kim, B.-M., Lim, G.-H., & Kim, K.-Y. A new look at the midlatitude-MJO teleconnection in the northern hemisphere winter. *Quart. J. Roy. Meteor. Soc.* **132,** 485–503 (2006).

23. Seo, K.-H. & Son, S.-W. The global atmospheric circulation response to tropical diabatic heating associated with the Madden–Julian oscillation during northern winter. *J. Atmos. Sci.* **69,** 79–96 (2012).

24. Loosmore, G. A. & Cederwall, R. T. Precipitation scavenging of atmospheric aerosols for emergency response applications: testing and updated model with new real-time data. *Atmos. Environ.* **38,** 993–1003 (2004).

25. Chen, Z. *et al.* Influence of meteorological conditions on $PM_{2.5}$ concentrations across China: A review of methodology and mechanism. *Environ. Intern.* **139,** 105558 (2020).

26. Kim, H., Vitart, F. & Waliser, D. E. Prediction of the Madden-Julian Oscillation: A review. *J. Climate*, **31,** 9425–9443 (2018).

27. Jiang, X. *et al.* Fifty years of research on the Madden-Julian Oscillation: Recent progress, challenges, and perspectives. *J. Geophys. Res. Atmos.* **125,** e2019JD030911 (2020).

28. Qu, W.J. *et al.* Spatial distribution and interannual variation of surface PM_{10} concentrations over eighty-six Chinese cities. *Atmos. Chem. Phys.* **10,** 5641–5662 (2010).

29. Zhang, X. Y. *et al.* Characterization of soil dust aerosol in China and its transport and distribution during 2001 ACE-Asia: 1. Network observations. *J. Geophys. Res. Atmos.* **108,** 1984–2012 (2003).

30. Li, Y., Tang, Y., Fan, Z., Zhou, H. & Yang, Z. Assessment and comparison of three different air quality indices in China. *Environ. Eng. Res.* **23,** 21–27 (2018).

31. Zhong, M. *et al.* Air quality modeling with WRF-Chem v3.5 in East Asia: sensitivity to emissions and evaluation of simulated air quality. *Geosci. Model Dev.* **9,** 1201–1218 (2016).

32. Hersbach, H. & Dee, D. ERA5 reanalysis is in production. *ECMWF Newsletter*. **147,** 7 (2016).

33. Garfinkel, C. I., Feldstein, S. B., Waugh, D. W., Yoo, C. & Lee, S. Observed connection between stratospheric sudden warmings and the Madden-Julian Oscillation. *Geophys. Lett.* **39,** L18807, (2012).

316 34. Kiladis, G.N. *et al.* A comparison of OLR and circulation based indices for tracking the MJO. *Mon.*
317 *Wea. Rev.* **142,** 1697–1715 (2014).

Figure lists

Fig. 1: Winter PM_{10} concentration in East Asia. (**a**) Daily climatology, (**b**) standard deviation, and (**c**) the ratio of the 20–96 day filtered subseasonal standard deviation to a daily standard deviation.

Fig. 2: MJO-related PM_{10}, precipitation frequency, and OLR anomalies. Composite PM_{10} anomalies averaged over lag 6–10 days during MJO phases (**a**) 1–2 and (**b**) 5–6. Multiple counts of the same day are not allowed. Sample size is denoted at the top-right corner, and values that are statistically significant at the 95% confidence level are denoted with filled circles. (**c**, **d**) Same as (**a**, **b**) but for midlatitude precipitation frequency anomalies over 20° N to 50° N averaged over lag 6–10 days and tropical OLR anomalies from the equator to 20° N at lag 0 day. Values that are statistically significant at the 95% confidence level are dotted.

Fig. 3: Frequency distribution of station-averaged PM_{10} concentration. (**a)** Frequency distribution of all PM_{10} observations with a bin size of 5 μg m^{-3}. Black line represents the generalized extreme value distribution. Unfiltered data are used. (**b**) Same as (**a**) but for the PM_{10} from lag 6 to 10 days during MJO phases 1–2 (blue) and 5–6 (red). Mean and one standard deviation are indicated at the top with dot and horizontal error bar, respectively.

Fig. 4: Atmospheric circulation anomalies during MJO phase 5–6. Composite anomalies of (**a**) 500-hPa geopotential height (shading) and wind (vectors), (**b**) bulk stability which is defined as potential temperature difference between 925 hPa and 1000 hPa, and (**c**) 10-m wind speed averaged over lag 6–10 days during MJO phase 5–6. Dotted areas and black arrows denote statistically significant values at the 95% confidence level.

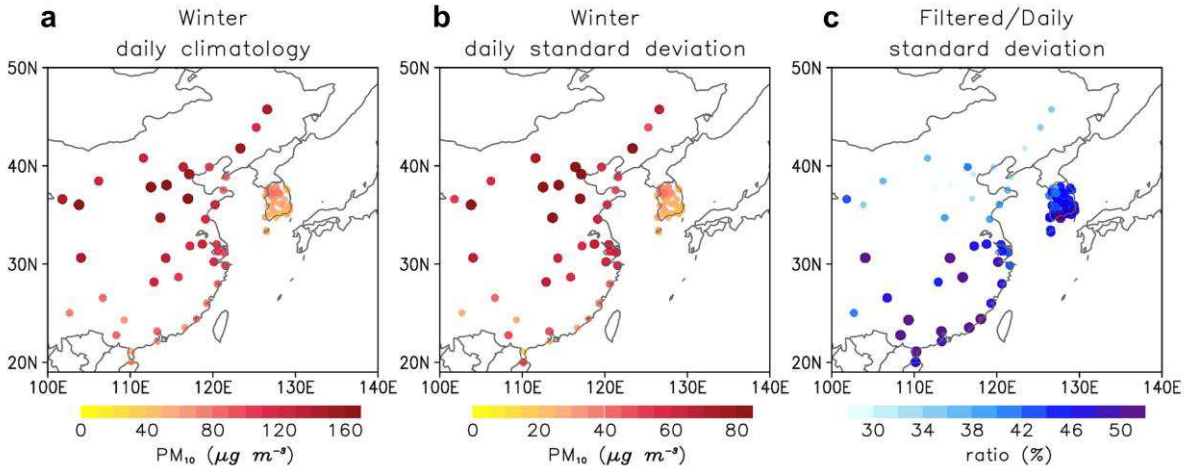

343

344 **Fig. 1: Winter PM_{10} concentration in East Asia.** (**a**) Daily climatology, (**b**) standard deviation, and (**c**)

345 the ratio of the 20–96 day filtered subseasonal standard deviation to a daily standard deviation.

346

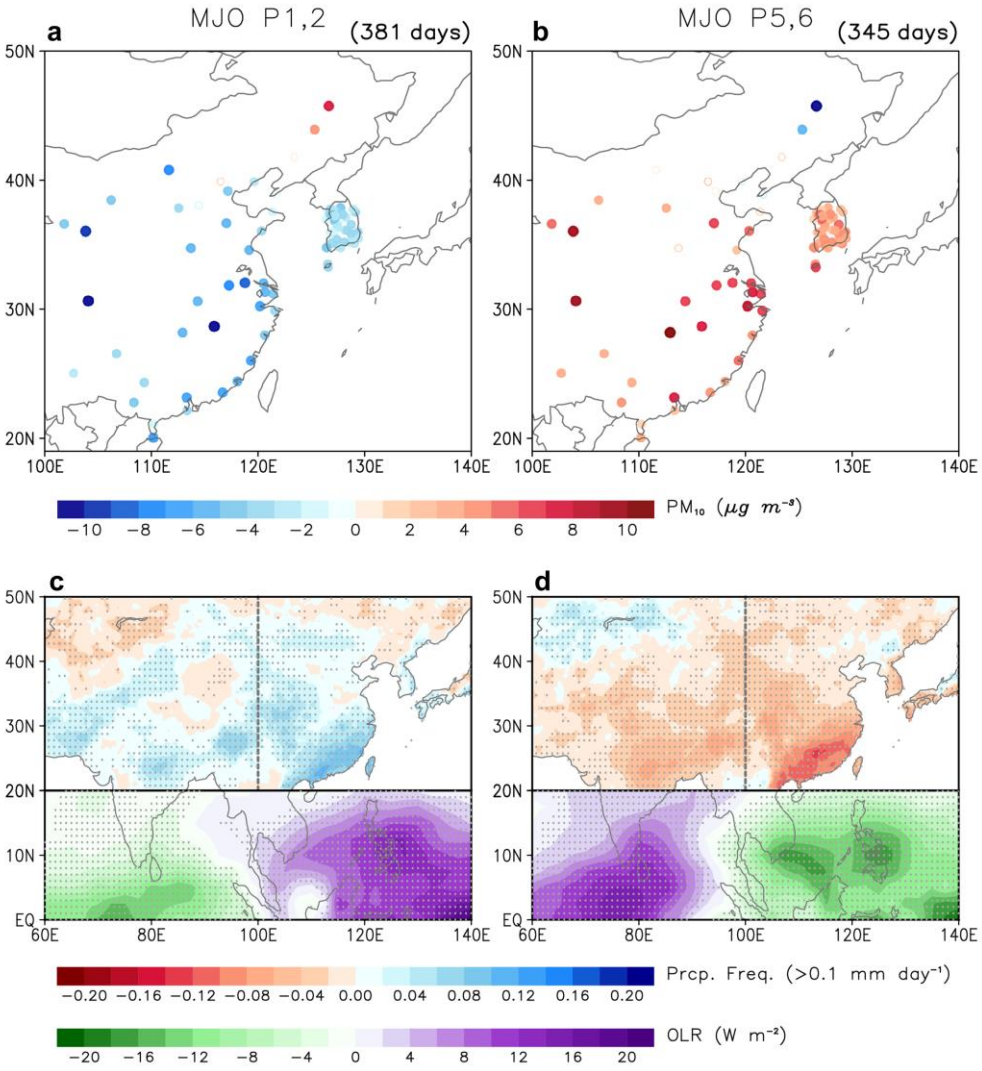

Fig. 2: MJO-related PM_{10}, precipitation frequency, and OLR anomalies. Composite PM_{10} anomalies averaged over lag 6–10 days during MJO phases (**a**) 1–2 and (**b**) 5–6. Multiple counts of the same day are not allowed. Sample size is denoted at the top-right corner, and values that are statistically significant at the 95% confidence level are denoted with filled circles. (**c**, **d**) Same as (**a**, **b**) but for midlatitude precipitation frequency anomalies over 20° N to 50° N averaged over lag 6–10 days and tropical OLR anomalies from the equator to 20° N at lag 0 day. Values that are statistically significant at the 95% confidence level are dotted.

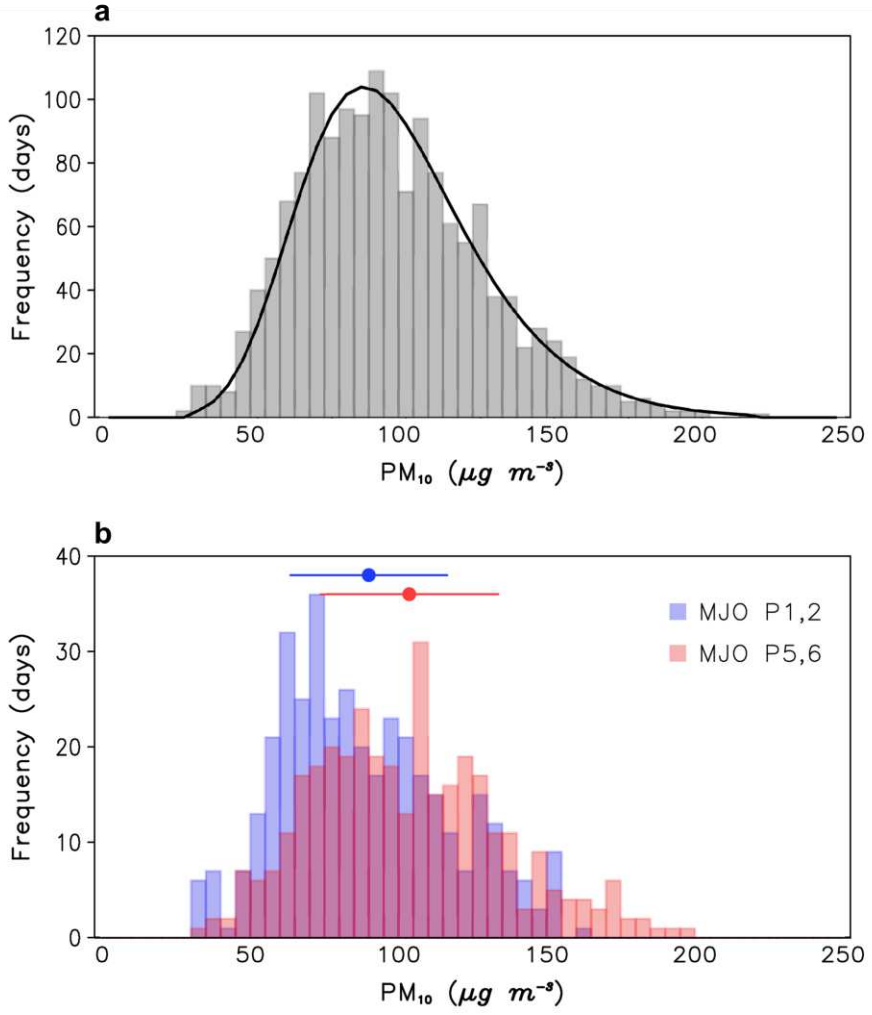

356

357 **Fig. 3: Frequency distribution of station-averaged PM_{10} concentration.** (**a**) Frequency distribution of
358 all PM_{10} observations with a bin size of 5 μg m^{-3}. Black line represents the generalized extreme value
359 distribution. Unfiltered data are used. (**b**) Same as (**a**) but for the PM_{10} from lag 6 to 10 days during MJO
360 phases 1–2 (blue) and 5–6 (red). Mean and one standard deviation are indicated at the top with dot and
361 horizontal error bar, respectively.

362

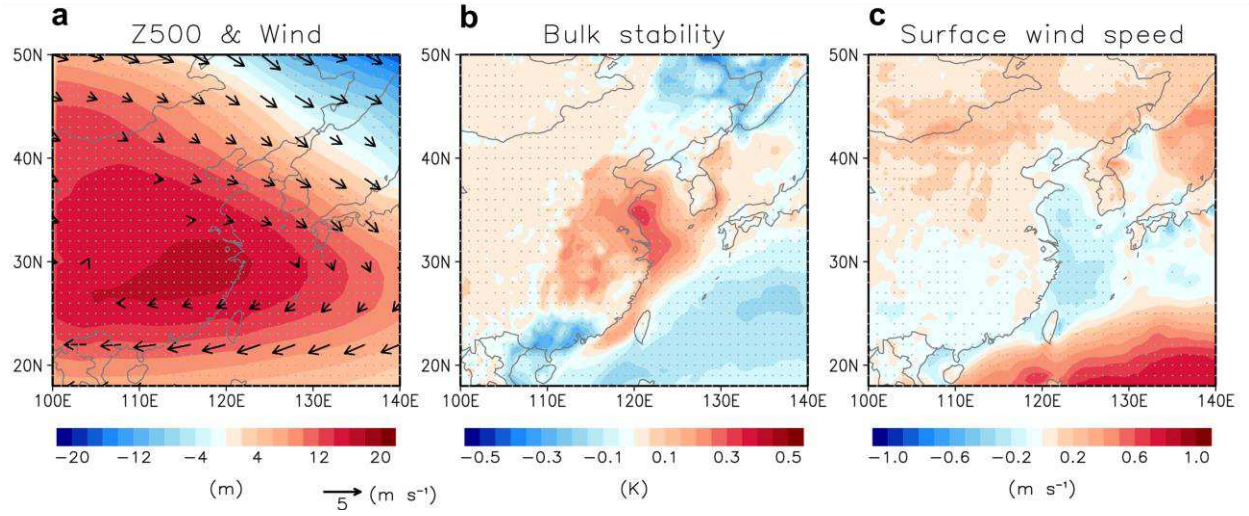

Fig. 4: Atmospheric circulation anomalies during MJO phase 5–6. Composite anomalies of (**a**) 500-hPa geopotential height (shading) and wind (vectors), (**b**) bulk stability which is defined as potential temperature difference between 925 hPa and 1000 hPa, and (**c**) 10-m wind speed averaged over lag 6–10 days during MJO phase 5–6. Dotted areas and black arrows denote statistically significant values at the 95% confidence level.

Figures

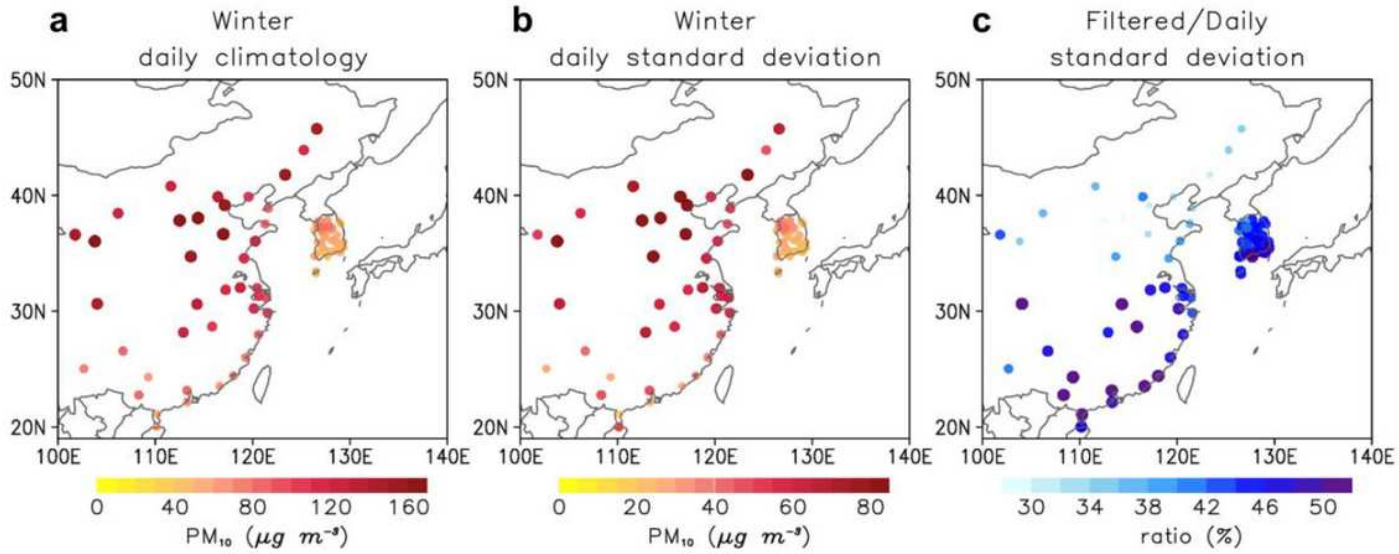

Figure 1

Winter PM10 concentration in East Asia. (a) Daily climatology, (b) standard deviation, and (c) the ratio of the 20–96 day filtered subseasonal standard deviation to a daily standard deviation.

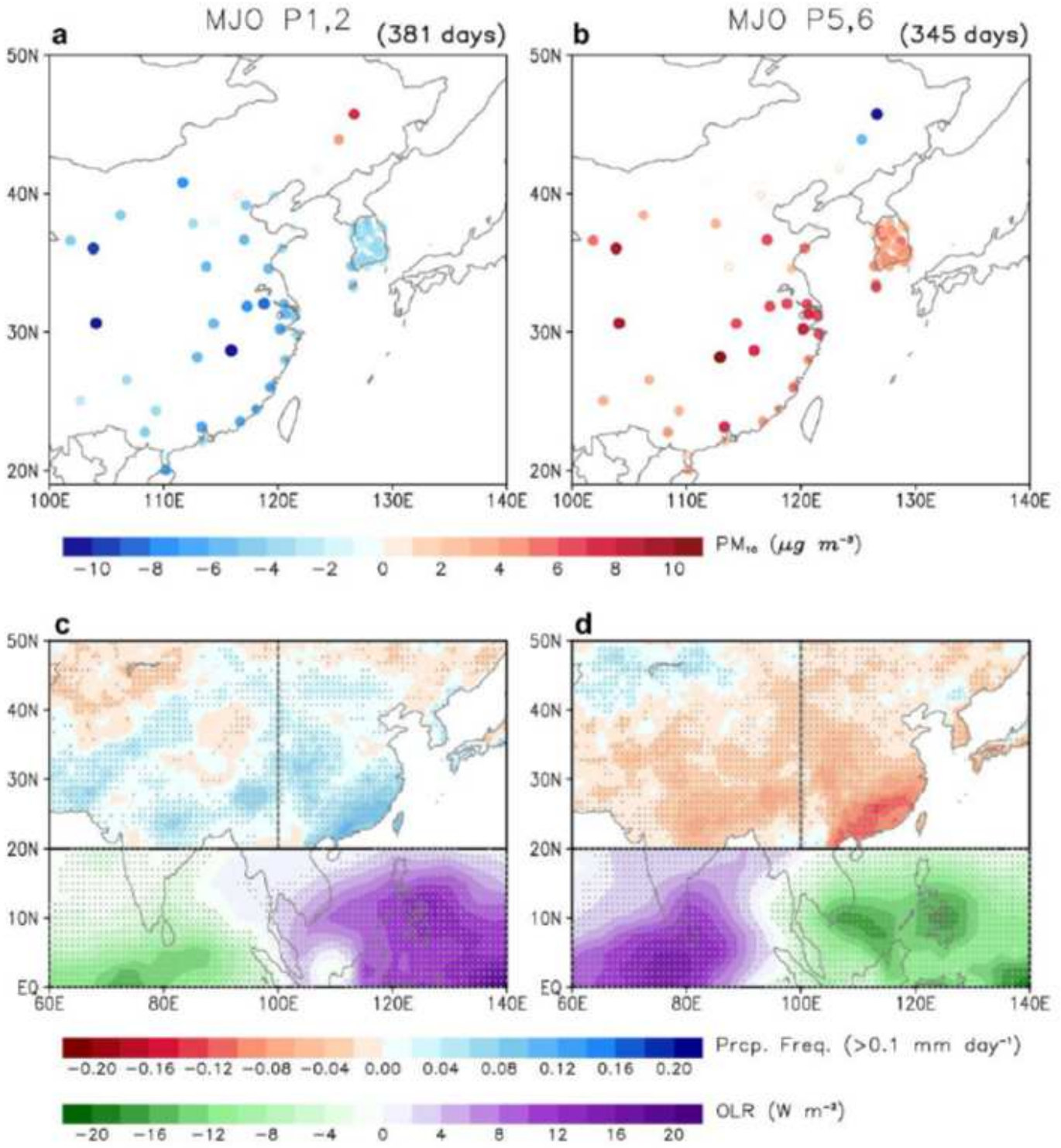

Figure 2

MJO-related PM10, precipitation frequency, and OLR anomalies. Composite PM10 anomalies averaged over lag 6–10 days during MJO phases (a) 1–2 and (b) 5–6. Multiple counts of the same day are not allowed. Sample size is denoted at the top-right corner, and values that are statistically significant at the 95% confidence level are denoted with filled circles. (c, d) Same as (a, b) but for midlatitude precipitation frequency anomalies over 20° N to 50° N averaged over lag 6–10 days and tropical OLR anomalies from

the equator to 20° N at lag 0 day. Values that are statistically significant at the 95% confidence level are dotted.

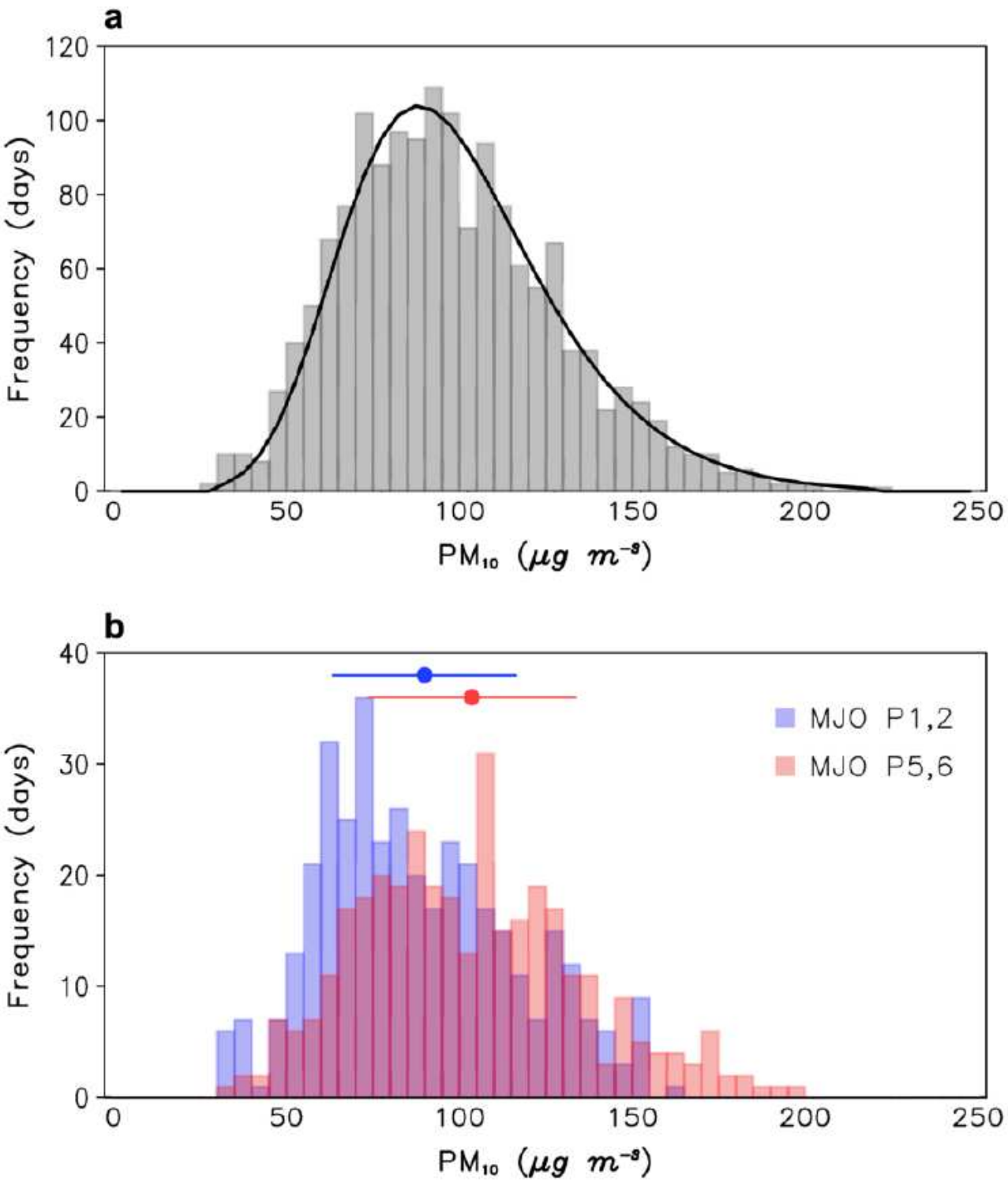

Figure 3

Frequency distribution of station-averaged PM10 concentration. (a) Frequency distribution of all PM10 observations with a bin size of 5 μg m-3. Black line represents the generalized extreme value distribution. Unfiltered data are used. (b) Same as (a) but for the PM10 from lag 6 to 10 days during MJO phases 1–2

(blue) and 5–6 (red). Mean and one standard deviation are indicated at the top with dot and horizontal error bar, respectively.

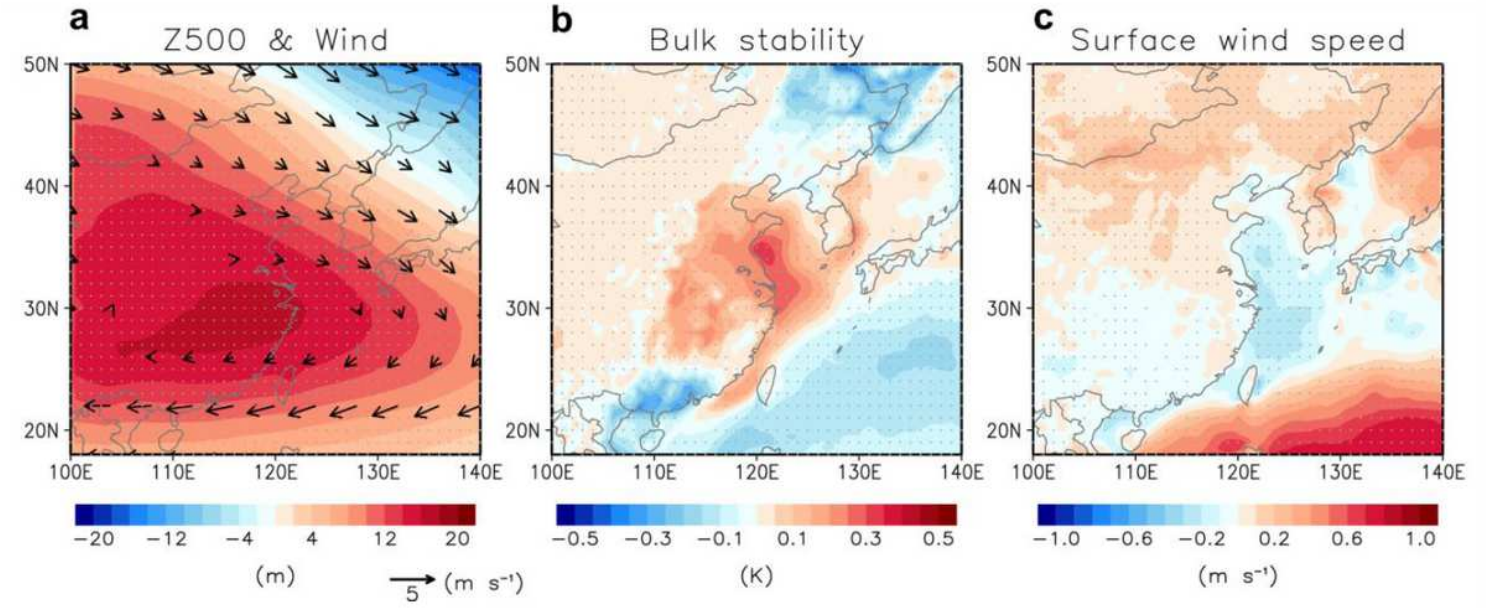

Figure 4

Atmospheric circulation anomalies during MJO phase 5–6. Composite anomalies of (a) 500-hPa geopotential height (shading) and wind (vectors), (b) bulk stability which is defined as potential temperature difference between 925 hPa and 1000 hPa, and (c) 10-m wind speed averaged over lag 6–10 days during MJO phase 5–6. Dotted areas and black arrows denote statistically significant values at the 95% confidence level.

Supplementary Files

This is a list of supplementary files associated with this preprint. Click to download.

- ExtendedData.pdf